

# Lanthanide(III) Metal-Organic Frameworks (Ln = Gd, Tb, Dy) Based on a C<sub>3</sub> Symmetrical Tricarboxylate Linker

Darragh McHugh,<sup>[a, b]</sup> Wenming Tong,<sup>[b]</sup> Andrey Bezrukov,<sup>[a, c]</sup> Pau Farras,<sup>[b]</sup> Michael J. Zaworotko,<sup>[a, c]</sup> Julia Mayans,<sup>[d]</sup> Jonathan M. Skelton,<sup>[e]</sup> Sarah Barnett,<sup>[f]</sup> Anuradha R. Pallipurath,<sup>[g]</sup> and Constantina Papatriantafyllopoulou<sup>\*[a, b]</sup>

*In loving memory of Professor Pat McArdle—a brilliant scientist, inspiring mentor, and kind colleague*

Lanthanide-based metal-organic frameworks have attracted significant interest due to their ability to combine porosity with one or more additional properties, providing an alternative method for the development of multifunctional materials. With this in mind, we report the synthesis and characterisation of the **OnG5** family of MOFs with the formula [LnL<sub>H</sub>(DMF)<sub>3</sub>][(4-NH<sub>2</sub>Ph)<sub>3</sub>C](NO<sub>3</sub>)(CH<sub>3</sub>CO<sub>2</sub>H), where Ln = Gd (**OnG5-Gd**), Tb (**OnG5-Tb**), Dy (**OnG5-Dy**), and L<sub>H</sub><sup>3-</sup> = the trianion of 4,4',4''-(1 E)-[4,4',4''-(methanetriyl)tris(benzene-4,1-diyl)tris(azan-1-yl-1-ylidene)]tris(methan-1-yl-1-ylidene)tribenzoic acid. **OnG5** were synthesised *in situ* from the reaction of Ln(NO<sub>3</sub>)<sub>3</sub>·xH<sub>2</sub>O, para-

rosaniline base [(4-NH<sub>2</sub>Ph)<sub>3</sub>COH] and terephthalaldehydic acid in DMF. Their structure was studied through single crystal x-ray crystallography and confirmed with DFT calculations. **OnG5** display a 2D, three-fold interpenetrated structure with a honeycomb lattice topology. They are the first examples bearing the ligand L<sub>H</sub>H<sub>3</sub> and they display photoluminescence originating from an intraligand π-π\* or n-π\* transition. *Dc* and *ac* magnetic susceptibility studies conducted on the **OnG5-Gd** analogue revealed an absence of magnetic interaction between the metal centres.

## Introduction

Multifunctional metal-organic frameworks (MOFs) have attracted significant research interest in recent years primarily due to their high porosity and large surface area, which make them suitable for a variety of applications.<sup>[1–5]</sup> These materials combine porosity with properties such as magnetism<sup>[6,7]</sup> or photoluminescence,<sup>[8,9]</sup> while their tuneable structures allow for

the design of new species with tailored functionalities. Multifunctional MOFs have been extensively studied in catalysis, sensing, photonics, and biomedical applications, including theranostics and drug delivery. They offer platforms for combined cancer treatments that integrate chemotherapy with methods like phototherapy, immunotherapy, and radiotherapy.<sup>[10–19]</sup> Furthermore, the synergistic effect between different properties often enhances their performance. While 3D multifunctional MOFs generally offer higher porosity and surface area, 2D MOFs are equally important as they allow easier access to active sites, thus improving reaction kinetics in catalytic reactions.<sup>[9,10]</sup>

A subclass of multifunctional MOFs involves lanthanide MOFs (Ln-MOFs).<sup>[20–36]</sup> The introduction of a Ln<sup>III</sup> ion into a MOF structure has the potential to result in the isolation of a material that accentuates the intrinsic luminescent and/or magnetic properties of Ln's while retaining the advantageous high crystallinity, and porosity of MOF. Concerning the luminescent properties of Ln-MOFs, the rigidity of their framework limits the linkers in a manner not commonly found in free complexes in solution, which promotes increased fluorescence lifetimes and quantum efficiencies.<sup>[21,25–28]</sup> Moreover, the emission of Ln-MOFs is influenced by the presence of guest molecules, which in turn can cause changes in intensity, wavelength, or even create new emissions, enabling them to operate as sensors for different analytes.<sup>[22,27–30]</sup> In addition to fluorescence properties, most Ln<sup>III</sup> ions combine large single-ion anisotropy with large large ground spin state values (*S*). This inherent magnetism has led to exploration of integrating Ln<sup>III</sup> ions into MOFs to create materials that can exhibit single molecule magnetism

[a] D. McHugh, A. Bezrukov, M. J. Zaworotko, C. Papatriantafyllopoulou  
SSPC Research Ireland Centre for Pharmaceuticals

[b] D. McHugh, W. Tong, P. Farras, C. Papatriantafyllopoulou  
School of Biological and Chemical Sciences, College of Science and  
Engineering, University of Galway, H91 TK 33 Galway, Ireland  
E-mail: constantina.papatriantafylopo@universityofgalway.ie

[c] A. Bezrukov, M. J. Zaworotko  
Department of Chemical Sciences, Bernal Institute, University of Limerick,  
Limerick, V94T9PX, Republic of Ireland

[d] J. Mayans  
Departament de Química Inorgànica i Orgànica, Secció Inorgànica and  
Institute of Nanoscience (IN2UB) and Nanotechnology, Universitat de  
Barcelona, Martí i Franques 1–11, Barcelona 08028, Spain

[e] J. M. Skelton  
School of Chemistry, University of Manchester, Manchester M13 9PL, UK

[f] S. Barnett  
Diamond Light Source, Harwell Science and Innovation Campus, Didcot  
OX11 0DE, UK

[g] A. R. Pallipurath  
School of Chemical and Process Engineering, University of Leeds, Leeds, UK

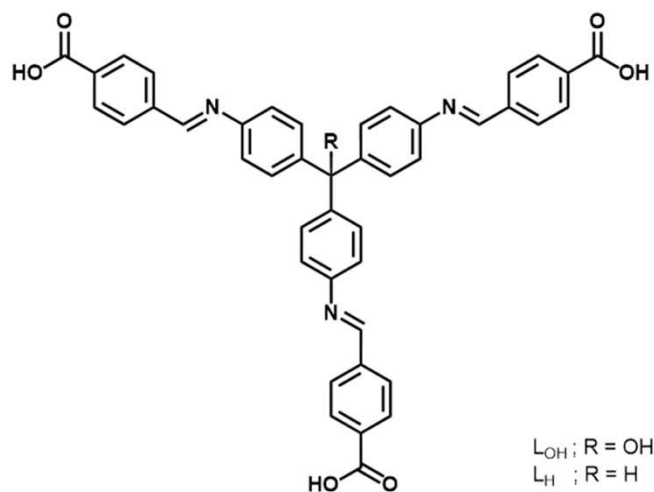
© 2024 The Author(s). European Journal of Inorganic Chemistry published by Wiley-VCH GmbH. This is an open access article under the terms of the Creative Commons Attribution License, which permits use, distribution and reproduction in any medium, provided the original work is properly cited.

(SMM)<sup>[20,31–33]</sup> behaviour and can be used as magnetic sensors, or as T1-weighted contrast agents in magnetic resonance imaging (MRI), where T1 refers to the longitudinal relaxation time. Recently, Gd-MOFs have shown great potential as multi-modal theranostic materials.<sup>[34–36]</sup>

Besides their intriguing physical properties, lanthanide ions possess large coordination numbers, which enhances the stability of their compounds across various solvents, air, and reaction conditions. This stability is crucial not only for the applications of Ln-MOFs but also for designing MOFs with specific functionalities. In particular, the high stability, paired with weakly bound solvent molecules that can be easily removed, facilitates post-synthetic modifications and structural fine-tuning.<sup>[37–39]</sup> This capability introduces significant synthetic control and allows for targeted synthesis.

Among various types of Ln-MOFs, those exhibiting high porosity are particularly significant as they can encapsulate large biomolecules and/or drugs. However, the low stability of MOFs with large pores poses a main synthetic challenge. To address this, elongated polytopic rigid linkers that promote strong coordination bonds are used to construct robust structures, preventing the decomposition of the constituent organic linker. Typically, these linkers are aromatic phenylene or acetylene-based, paired with carboxylate moieties known for their strong binding capabilities.<sup>[40]</sup> To this end, several synthetic methods have been investigated for Ln-MOFs, including solvothermal methods, precipitation, ultrasonic synthesis, post-synthesis modification, and isorecticular expansion.<sup>[24]</sup> This has led to the isolation of numerous Ln MOFs with diverse topologies, some of which interestingly combining more than two properties.<sup>[20,31]</sup> A prime such example is the family of MOF with the formula  $\{[Ln_3L_6(OH)_3(DMF)_3] \cdot 5H_2O\}_n$ , where  $H_2L = 3$ -amino-4-hydroxybenzoic acid ligand.<sup>[20]</sup> These MOFs exhibit intriguing characteristics such as single-molecule magnetism and notable photoluminescence properties. Additionally, their porosity enables CO<sub>2</sub> encapsulation.

With the above in mind, we decided to expand the family of Ln-MOFs using 4,4',4''-(1 E)-[4,4',4''-(hydroxymethanetriyl)tris(benzene-4,1-diyl)tris(azan-1-yl-1-ylidene)]tris(methan-1-yl-1-ylidene)tribenzoic acid ( $L_{OH}H_3$ , Scheme 1) as the organic linker. This ligand has previously been used by Tasiopoulos research group to synthesise a double-interpenetrated Zn-based MOF that exhibits a large surface area and high CO<sub>2</sub> uptake, but its employment in Ln<sup>III</sup> chemistry is unexplored.<sup>[41]</sup> Herein, the synthesis of the ligand was attempted *in situ* from the Schiff base reaction between parosaniline base [(4-NH<sub>2</sub>Ph)<sub>3</sub>COH] and terephthalaldehydic acid in an acidic environment, which favoured the loss of the hydroxyl group in the tris(P-aminophenyl)methanol, resulting in a virtually planar carbocationic (methylum) system [(4-NH<sub>2</sub>Ph)<sub>3</sub>C]<sup>+</sup> and the formation of the ligand  $L_HH_3$  (Scheme 1).<sup>[42]</sup> This reaction led to the synthesis of the **OnG5** family of MOFs, where **OnG** stands for *Ollscoil na Gaillimhe* (University of Galway). The MOFs possess the formula  $[LnL_H(DMF)_3][(4-NH_2Ph)_3C](NO_3)(CH_3CO_2H)$ , where Ln = Gd (**OnG5-Gd**), Tb (**OnG5-Tb**), Dy (**OnG5-Dy**), and display a 2D structure and a honeycomb lattice topology. These are the first examples



**Scheme 1.** Schematic representation of the ligands  $L_{OH}$  and  $L_H$  discussed in the text.

bearing the ligand  $L_HH_3$ . The crystal structures and properties of **OnG5** have been studied with a variety of techniques, including, single crystal and powder x-ray diffractometry, thermal stability, photoluminescence, computational and magnetism studies.

## Results and Discussion

### Synthesis

Our group has been focusing on the synthesis and characterisation of new MOFs with drug delivery or sensing properties. This work has led to the isolation of a variety of different 3 d metal ion-based homometallic and heterometallic MOFs with new topologies and properties. Representative such examples are the **NUIG1** and **NUIG4** MOFs, which can encapsulate an unexpectedly large amount of NO, ibuprofen, and doxorubicin.<sup>[43–45]</sup> **NUIG1** can also act as magnetism-based sensor for environmentally toxic species, with its magnetic properties being affected by the type and quantity of encapsulated molecules.<sup>[44]</sup> To further this research and investigate the potential of isolating multifunctional MOFs, we incorporated Ln<sup>III</sup> ions into the reaction system to leverage their photoluminescence and magnetism properties.

Several experiments were conducted to investigate the effect of synthetic parameters, such as temperature, reagent ratios, solvents and other reaction conditions. The reaction of  $Ln(NO_3)_3 \cdot xH_2O$  (Ln = Gd, **OnG5-Gd**; Tb, **OnG5-Tb**; Dy, **OnG5-Dy**), parosaniline base [(4-NH<sub>2</sub>Ph)<sub>3</sub>COH] and terephthalaldehydic acid in a 1:1.7:4.2 reaction ratio in DMF at 100 °C resulted in round dome-shaped crystals of  $[LnL_H(DMF)_3][(4-NH_2Ph)_3C](NO_3)(CH_3CO_2H)$  in good yield. Acetic acid was added as modulator and improved the crystallinity of the product. Simultaneously, the combination of acetic acid and terephthalaldehydic acid created an acidic environment, favouring the formation of the carbocation  $[(4-NH_2Ph)_3C]^+$ . Parosaniline

base is known to be unstable in acidic environments, readily releasing the hydroxyl group.<sup>[42,46]</sup>

It is worth mentioning that *in-situ* synthesis was used to produce the family of **OnG5** MOFs while preliminary one-step reactions with pre-synthesised ligand resulted in amorphous products. The synthesis is sensitive to the ratio of reagents with small variations in this ratio leading to the formation of amorphous or microcrystalline products that cannot be characterised further.

### Description of Structures

**OnG5** MOFs display related structures, differing in the type of Ln<sup>III</sup> (Ln = Gd, **OnG5-Gd**; Tb, **OnG5-Tb**; Dy, **OnG5-Dy**). The structure of **OnG5-Gd** is discussed in detail below. Representation of the molecular structure of the **OnG5-Gd** is shown in Figures 1, 2, and S1–S5 in the SI. Details of bond distances and angles, as well as crystallographic information are shown in Tables S1–S5 in the SI.

**OnG5-Gd** crystallises in the hexagonal space group P63 (unit cell parameters:  $a = 13.8952(1)$  Å,  $b = 13.8952(1)$  Å,  $c = 21.3255(2)$  Å), consisting of a polymeric network based on the repeating unit  $[\text{GdL}_n(\text{DMF})_3](4\text{-NH}_2\text{Ph})_3\text{C}^+(\text{NO}_3)(\text{CH}_3\text{CO}_2\text{H})$ , nitrate ion,  $[(4\text{-NH}_2\text{Ph})_3\text{C}]^+$  carbocation, and disordered acetic acid inclusion (Figure 1). The coordination sphere of the Gd ion is completed by three chelate bidentate carboxylate groups, which come from three different linkers. The latter are in their trianionic form and adopt an  $\eta^1:\eta^1:\eta^1:\eta^1:\eta^1:\mu_3$  coordination mode linking three neighbouring building units.

The Gd ions are nine-coordinate. To determine the coordination polyhedra around Gd1, the experimental structural data were compared with theoretical data for common polyhedral structures with 9 vertices using the SHAPE software.<sup>[47,48]</sup> The main semi-regular three-dimensional figures considered were the octagonal pyramid, the heptagonal bipyramid, and five Johnson polyhedra (capped cube, capped square antiprism, tricapped trigonal prism, tridiminished icosahedron, triangular cupola). The best match was found for a tricapped trigonal prism.

The structure of **OnG5-Gd** is interpenetrated consisting of three interwoven nets in a honeycomb lattice topology (*hcb*) in 3-c uninodal net (Figure 1, bottom).<sup>[49–51]</sup> The neighbouring layers in **OnG5-Gd** are well-separated with their distance being 33.0(2) Å. The  $\text{NO}_3^-$  and  $[(4\text{-NH}_2\text{Ph})_3\text{C}]^+$  ions are positioned above and below the polymeric layers (Fig. 2). They are in close proximity to the framework, with a distance of 4.925 Å between the  $\text{NH}_2$  groups of  $[(4\text{-NH}_2\text{Ph})_3\text{C}]^+$  and the Gd atom, suggesting a very subtle interaction between the carbocation and the lanthanide. The closest metal metal distance is 13.9(2) Å between Gd ions within the same layer. The honeycomb topology is common in MOFs.<sup>[49–51]</sup> A notable example is the Sc(III)-based MOF **CCIQS-1**, which contains 4,4'-(9,10-anthracenediyl)dibenzoate ligands.<sup>[49b]</sup> Similar to **OnG5**, **CCIQS-1** features a three-fold interpenetrated hexagonal honeycomb network structure, and exhibits reversible porosity changes that adapt to guest molecule size and polarity.

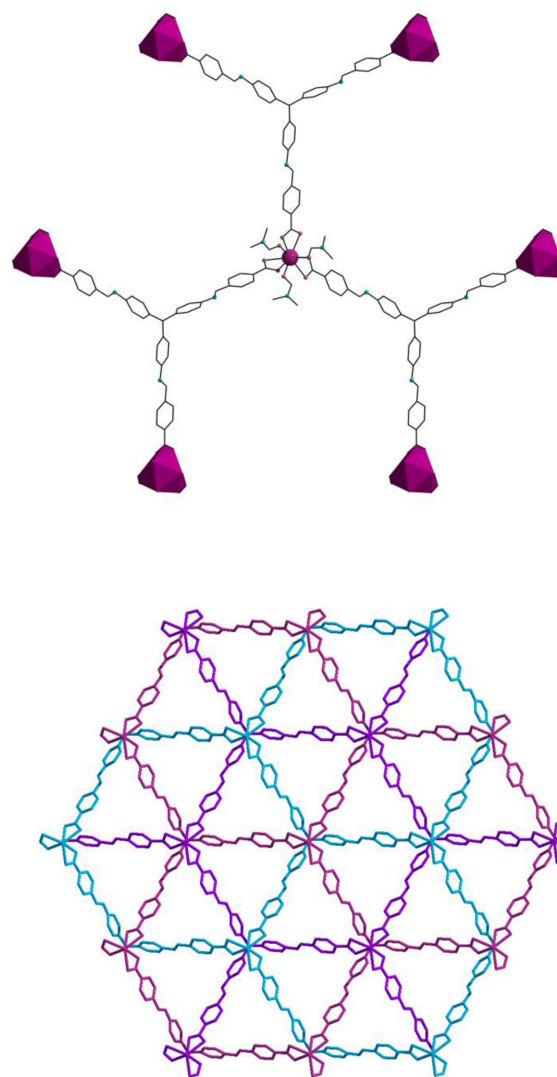


**Figure 1.** Top : Representation of the SBU and ligand connectivity in **OnG5-Gd**. Colour code: N, blue; Gd, magenta; O, red; C, grey. Hydrogen atoms and lattice ions are omitted for clarity. Bottom: The three interwoven nets in **OnG5**, each shown in different colour.

The crystal structure of **OnG5** is stabilised through intermolecular interactions. The  $\text{NH}_2$  groups (N2, Figure S1) of the carbocation  $[(4\text{-NH}_2\text{Ph})_3\text{C}]^+$  act as donors in two distinct hydrogen bonding interactions: the first with the O atoms of the  $\text{NO}_3^-$  ions (O4, Figure S1), and the second with O2 from coordinated carboxylate groups ( $\text{N2}\cdots\text{O2} = 2.891(5)$  Å,  $\text{H2 A}\cdots\text{O2} = 1.989(5)$  Å,  $\text{N2-H2 A}\cdots\text{O2} = 141.34(8)^\circ$ ). The aromatic rings of the  $[(4\text{-NH}_2\text{Ph})_3\text{C}]^+$  further interact with the aromatic rings of the coordinated ligand  $\text{L}_n^{3-}$  through weak  $\pi$ - $\pi$  stacking interactions; the distance between the centroids is 4.2 Å.

Pore analysis of the crystal structure carried out using the Mercury software suggested that, of the  $3557.687$  Å<sup>3</sup> system volume only  $403.401$  Å<sup>3</sup> was accessible to a Helium probe through 2D-networks. The limiting pore diameter used was 1.20 Å. Figure S6 depicts these pores through the void space representation in Mercury software.

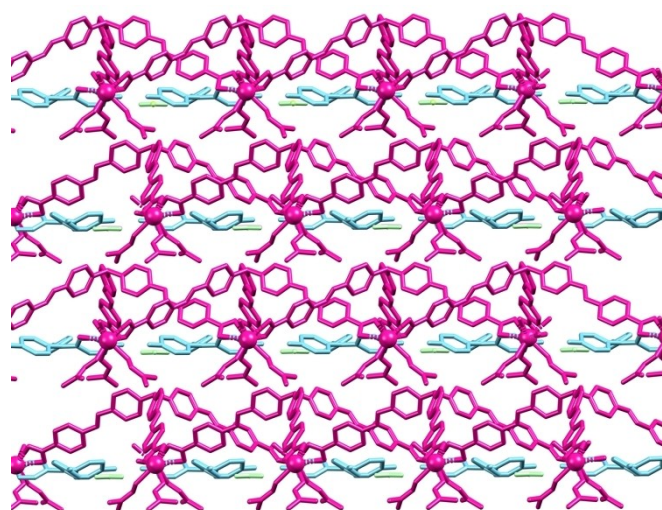


**Figure 2.** Representation of the crystal structure of **OnG5-Gd** featuring the  $\text{NO}_3^-$  and  $[(4\text{-NH}_2\text{Ph})_3\text{C}]^+$  ions positioned above and below the polymeric  $[\text{GdL}_\text{H}(\text{DMF})_3]$  layers. Colour code:  $[\text{GdL}_\text{H}(\text{DMF})_3]$ , magenta;  $[(4\text{-NH}_2\text{Ph})_3\text{C}]^+$ , cyan;  $\text{NO}_3^-$ , green.

The stability of **OnG5-Gd** was confirmed through thermal stability studies (Figure S7, SI). The compound decomposes in multiple steps, as expected due to the variety of ligands present in its structure. A mass loss of about 5.0% occurs up to 100 °C, which matches well with the expected mass from the release of the  $\text{CH}_3\text{CO}_2\text{H}$  in the lattice (expected value: 4.0%). There is a mass loss of approximately 15% between 100–250 °C, which is attributed to the weakly bound DMF molecules. The theoretical value is 14.92%. This is followed by a plateau, potentially attributable to a stable intermediate  $[\text{GdL}_\text{H}][(4\text{-NH}_2\text{Ph})_3\text{C}](\text{NO}_3)$ .

## Computational Studies

Ab initio density functional theory (DFT) optimisation was carried out on a bound Gd complex centre with two of the tridentate ligand terminations capped with carboxylic acid to terminate the polymeric repeating unit for the purposes of the calculation. The resultant structure agreed with the X-ray single crystal structure. The difference as can be seen in Figure S8, is that the tridentate ligand has moved by 0.357 Å and the phenyl rings attached to the C centre have twisted out-of-plane, rendering the whole ligand planar. The loss of planarity in the ligand in the crystal structure of **OnG5** is due to the tetrahedral geometry of the central C atom in the  $\text{C}_3$  symmetrical  $\text{L}_\text{H}\text{H}_3$  ligand. The simulated IR spectrum also agrees with the experimental data. The disordered acetic acid present in the crystallographic special position was removed during the calculations but the experimental spectrum also showed peaks related to acetic acid as confirmed from the spectrum from NIST database (Figure S9).

## Photoluminescence Studies

The solid-state emission spectra of the **OnG5** MOFs and the ligand were recorded at room temperature. Upon excitation at 220 nm, the emission spectra of the **OnG5** MOFs are identical to that of the ligand, showing emission peaks at 488 nm, 524 nm, 542 nm, 571 nm, and 600 nm (Figure 3). The observed photoluminescence in this case is likely originating from an intraligand  $\pi\text{-}\pi^*$  or  $\text{n-}\pi^*$  transition.

The photo-antenna effect is crucial for enhancing the emission of Ln ions.<sup>[52]</sup> This enhancement is achieved through intramolecular energy transfer, which is initiated by the photo-excitation of chromophores ligands via chemical bonding. In the case of **OnG5** MOFs, no fluorescence was observed due to the presence of lanthanides. This lack of fluorescence can be attributed to the poor sensitising effect of the ligand, which is caused by the absence of strong electron donor groups (e.g.  $\sigma$ -donors) that could enhance energy transfer. Additionally, the flexibility of the ligand and the presence of the carbocation or potential solvents in the structure may introduce non-radiative deactivation pathways through the coupling of the excited states of  $\text{Ln}^{3+}$  to matrix vibrations.

## Magnetism Studies

The  $\chi_{\text{MT}}$  vs.  $T$  measurements between 300–2 K for **OnG5-Gd** exhibit an almost perfect Curie law behaviour with a constant value of  $7.750 \text{ cm}^3 \text{ mol}^{-1} \text{ K}$  down to 2 K; this is close to the theoretical value of  $7.875 \text{ cm}^3 \text{ mol}^{-1} \text{ K}$  for an isolated  $S=7/2$ , suggesting no magnetic interaction between the  $\text{Gd}^{\text{III}}$  ions in the network. This implies a good isolation of the paramagnetic centres (Figure 4). The experimental magnetization up to 5 T of the external magnetic field saturates at  $7.05 N\mu\beta$ , following a perfect Brillouin function going to 7 electrons.

Recent examples of  $\text{Gd}^{\text{III}}$  MOFs exhibit slow relaxation of the magnetization, a phenomenon of increasing importance in the application of quantum technologies to coordination

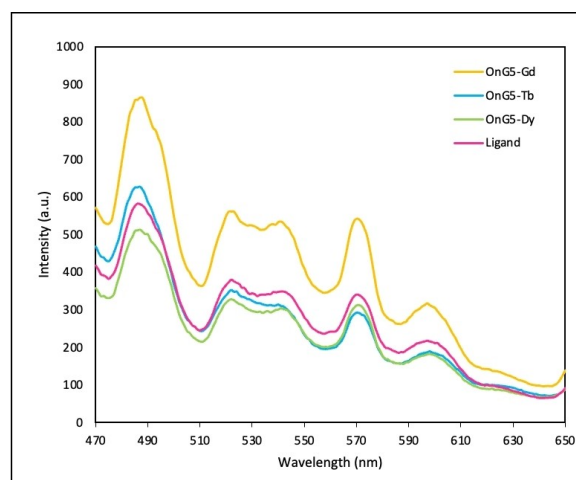


**Figure 3.** Emission spectrum of **OnG5-Gd** (Orange), **OnG5-Tb** (Blue), **OnG5-Dy** (Green) and ligand (Pink) upon excitation at 220 nm.

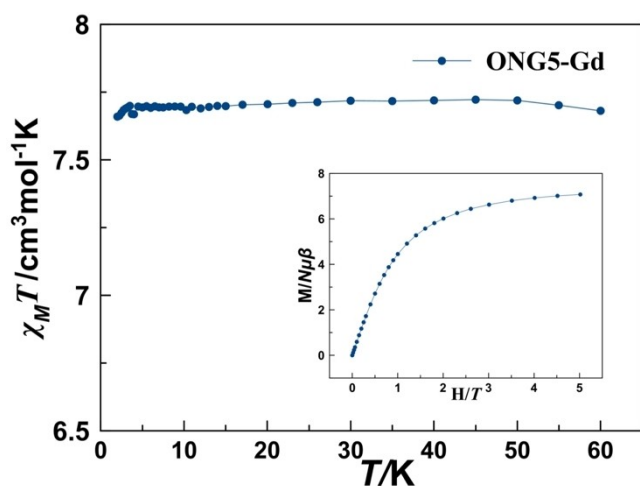


Figure 4. Susceptibility measurement for OnG5-Gd with a Curie law behaviour. Inset, magnetization curve up to 5 T.

compounds.<sup>[53,54]</sup> In this context, *ac* susceptibility measurements were performed on OnG5-Gd (Figure S10). However, in this case, probably due to the highly symmetric environment around the spin carrier, which does not allow the appropriate axial zero field splitting (*D*),<sup>[55]</sup> no slow relaxation response is observed.

## Conclusions

The initial use of the ligand 4,4',4''-(1 E)-[4,4',4''-(methanetriyl)tris(benzene-4,1-diyl)tris(azan-1-yl-1-ylidene)]tris(methan-1-yl-1-ylidene)tribenzoic acid ( $L_{\text{H}}H_3$ ) in Ln chemistry provided access to a new family of MOFs, namely  $[\text{Ln}L_{\text{H}}(\text{DMF})_3][(\text{4-NH}_2\text{Ph})_3\text{C}](\text{NO}_3)(\text{CH}_3\text{CO}_2\text{H})$  (Ln = Gd, OnG5-Gd; Tb, OnG5-Tb; Dy OnG5-Dy). OnG5 are the inaugural examples bearing the  $L_{\text{H}}H_3$  ligand. They were synthesised *in situ* from the reaction of a nitrate salt of the lanthanide ion, pararosanine base and terephthalaldehydic acid, and their structure can be described as a two-dimensional, three-fold interpenetrated framework in a honeycomb topology.

OnG5 exhibit photoluminescence arising from an intraligand  $\pi-\pi^*$  or  $n-\pi^*$  shift. *Ac* and *dc* magnetic susceptibility studies on OnG5 revealed that there are no interactions between the lanthanide ions, which aligns with the effective isolation of the latter. Moreover, due to the high symmetry in the coordination sphere of the lanthanide ions, the OnG5 MOFs do not display slow relaxation of magnetization.

This work highlights the potential of the ligand  $L_{\text{H}}H_3$  in facilitating the synthesis of new MOFs. Work is currently in progress for the isolation of three-dimensional species using pre-formed  $L_{\text{H}}H_3$  and  $L_{\text{OH}}H_3$  ligands (Scheme 1). This method avoids the incorporation of cations formed during *in-situ* synthesis, potentially resulting in MOFs with increased dimensionality and/or porosity.

## Experimental Section

All manipulations were performed under aerobic conditions using materials as received. Warning: Nitrate salts are potentially explosive; such compounds should be used in small quantities and treated with utmost care at all times.

### Synthesis of $[\text{Gd}L_{\text{H}}(\text{DMF})_3][(\text{4-NH}_2\text{Ph})_3\text{C}](\text{NO}_3)(\text{CH}_3\text{CO}_2\text{H})$ (OnG5-Gd)

$\text{Gd}(\text{NO}_3)_3 \cdot 6\text{H}_2\text{O}$  (0.049 g, 0.11 mmol), was added to a glass vial containing DMF/AcOH (5 ml, 50  $\mu\text{l}$ ) and magnetically stirred until dissolved. Upon dissolution, pararosanine base (0.062 g, 0.19 mmol) and terephthalaldehydic acid (0.069 g, 0.46 mmol) was added to the vial and magnetically stirred for a 5 min. The reaction was then capped and placed in the oven at 100 °C for 24 hours, yielding single crystals which were kept in their mother solution for x-ray analysis. Yield 25%. Anal. Calc. for OnG5-Gd: C, 59.66; H, 4.87; N, 9.53. Found: C, 60.12; H, 5.09; N, 9.97%. Selected IR data (KBr,  $\text{cm}^{-1}$ ): 3330 (m), 3169 (m), 2925 (w), 2723 (w), 2163 (w), 1999 (w), 1644 (s), 1576(s), 1414 (s), 1333 (s), 1162 (s), 1106 (s), 909 (m), 853 (s), 783 (m), 678 (s).

### Synthesis of $[\text{Tb}L_{\text{H}}(\text{DMF})_3][(\text{4-NH}_2\text{Ph})_3\text{C}](\text{NO}_3)(\text{CH}_3\text{CO}_2\text{H})$ (OnG5-Tb)

The synthesis of this analogue follows the same procedure as OnG5-Gd but using  $\text{Tb}(\text{NO}_3)_3 \cdot 5\text{H}_2\text{O}$  (0.049 g, 0.11 mmol). Yield 20%. Anal. Calc. for OnG5-Tb: C, 59.59; H, 4.86; N, 9.52. Found: C, 59.66; H, 5.24; N, 10.01%. Selected IR data (KBr,  $\text{cm}^{-1}$ ): 3330 (m), 3170 (m), 2981 (w), 2728 (w), 2203 (w), 1999 (w), 1645 (s), 1578 (s), 1415 (s), 1336 (s), 1165 (s), 1107 (s), 910 (m), 854 (s), 783 (m), 678 (s).

### Synthesis of $[\text{Dy}L_{\text{H}}(\text{DMF})_3][(\text{4-NH}_2\text{Ph})_3\text{C}](\text{NO}_3)(\text{CH}_3\text{CO}_2\text{H})$ (OnG5-Dy)

The synthesis of this analogue follows the same procedure as OnG5-Gd but using  $\text{Dy}(\text{NO}_3)_3 \cdot \text{H}_2\text{O}$  (0.049 g, 0.14 mmol). Yield 25%. Anal. Calc. for OnG5-Dy: C, 59.45; H, 4.85; N, 9.50. Found: C, 59.89; H, 4.96; N, 9.72%. Selected IR data (KBr,  $\text{cm}^{-1}$ ): 3328 (m), 3167 (m), 2927 (w), 2725 (w), 2000 (w), 1645 (s), 1577 (s), 1416 (s), 1333 (s), 1162 (s), 1106 (s), 909 (m), 853 (s), 783 (m), 678 (s).

## Physical Studies

Elemental analyses (C, H, N) were performed in-house at the University of Galway, School of Biological & Chemical Sciences. IR spectra ( $4000-400 \text{ cm}^{-1}$ ) were recorded using a Perkin Elmer 16PC FT-IR spectrometer. Solid-state, variable-temperature and variable-field magnetic data were collected on a powdered sample using an MPMS5 Quantum Design magnetometer operating at 0.03 T in the 300 to 2.0 K range for the magnetic susceptibility and at 2.0 K in the 0 to 5 T range for the magnetization measurements. The observed susceptibilities were corrected for diamagnetism using Pascal's constants.<sup>[56]</sup> TGA experiments were performed on a STA625 thermal analyzer from Rheometric Scientific (Piscataway, New Jersey). The heating rate was kept constant at 20 °C/min, and all runs were carried out between 20 and 600 °C. The measurements were made in open aluminum crucibles, and nitrogen was purged in ambient mode. Calibration was performed using an indium standard. Solid-state UV studies were carried out using an Agilent Cary 5000 UV-Vis-NIR spectrophotometer. Fluorimetry studies were conducted on an Agilent Cary Eclipse fluorescence spectrophotometer.

## X-ray Crystallography

Single crystal diffraction data for **OnG5-Gd** were collected at the I19-chemical crystallography beamline at Diamond light source. The data was collected using synchrotron radiation at  $\lambda=0.6889$  Å under ambient pressure and at 293(2) K.

The diffraction data was automatically integrated using the XIA2 program that runs the DIALS code. Data completeness of 100% to  $48.8^\circ 2\theta$  and 97% to  $74.2^\circ 2\theta$  to a distance of 0.81 Å was achieved.

The structure solution was attempted using the OLEX2 program,<sup>[57]</sup> with SHELXT<sup>[58]</sup> Intrinsic phasing method for the structure solution and SHELXL<sup>[58]</sup> with least squares method for the refinement. A solvent mask of 1.2 Å that truncates at 1.2 Å was used to squeeze the electrons. The U(iso) was fixed at 1.2 times for all C(H and the aromatic/amide Hs were refined using Riding co-ordinates. 78833 reflections were measured ( $3.284^\circ 2\theta \leq 72.368^\circ$ ), 11797 were unique ( $R_{\text{int}}=0.0443$ ,  $R_{\text{sigma}}=0.0301$ ) which were used in all calculations. The final R1 was 0.0402 ( $I > 2\sigma(I)$ ) and  $wR^2$  was 0.1249 (all data). The refined structure parameters are:  $C_{73}H_{66}GdN_{10}O_{12}$  ( $M=1432.60$  g/mol): hexagonal, space group P63 (no. 173),  $a=13.89520(10)$  Å,  $c=21.3255(2)$  Å,  $V=3565.82(6)$  Å<sup>3</sup>,  $Z=2$ ,  $T=100.15$  K,  $\mu=0.922$  mm<sup>-1</sup>,  $D_{\text{calc}}=1.334$  g/cm<sup>3</sup>.

The crystal structures of **OnG5-Tb** and **OnG5-Dy** were characterised by PXRD studies. Figure S11 shows that the experimental PXRD patterns for both MOFs match perfectly with **OnG5-Gd**, confirming the structural similarities of the **OnG5** MOFs.

Unit cell data and structure refinement details are listed in Table S1. The CIF file can be obtained free of charge at [www.ccdc.cam.ac.uk/retrieving.html](http://www.ccdc.cam.ac.uk/retrieving.html) or from the Cambridge Crystallographic Data Centre, Cambridge, UK with the REF code 237624.

## Ab Initio Structure Refinement

The solved X-ray structure was optimised with periodic density-functional theory (DFT) as implemented in the Vienna Ab initio Simulation Package (VASP) code.<sup>[59]</sup> Electron exchange and correlation were modelled with the PBE generalised-gradient approximation functional<sup>[60]</sup> with the DFT–D3 dispersion correction<sup>[61]</sup> (i.e. PBE + D3). The ion cores were modelled using projector augmented-wave (PAW) pseudopotentials.<sup>[62,63]</sup> For Gd, we used the Gd(III) potential which subsumes the unpaired f electrons in  $Gd^{3+}$  in the core, avoiding the difficulties of modelling such strongly-correlated electrons with semi-local DFT. This potential has nine electrons in the valence region. For the other elements, we used pseudopotentials with the following valence configurations: H -  $1s^1$ , C -  $2s^22p^2$ , N -  $2s^22p^3$ , and O -  $2s^22p^4$ . The atom positions were optimised to tight tolerances of 10–8 eV on the electronic total energy and  $10^{-2}$  eV Å<sup>-1</sup> on the forces, with the lattice parameters fixed to the experimental values. The precision of the charge-density grids were set automatically to avoid aliasing errors (PREC=Accurate in VASP), the PAW projection was performed in real space (LREAL=Auto), and non-spherical contributions to the gradient corrections inside the PAW spheres were fully accounted for (LASPH=.TRUE.). To simulate the infrared (IR) spectrum, the frequencies, eigenvectors and irreducible representations of the  $\Gamma$ -point phonon modes were obtained using the finite-difference approach implemented in the Phonopy code,<sup>[64]</sup> with the default step size of  $10^{-2}$  Å and without expanding the unit cell. These were then paired with the Born effective-charge tensors computed using the density-functional perturbation theory (DFPT) routines in VASP<sup>[65]</sup> to generate the IR spectrum using the Phonopy-Spectroscopy package.<sup>[66]</sup> For the single-point force calculations on displaced structures and the DFPT Born-charge calculations an additional support grid with 8x the number of points as

the standard grid was used to ensure accurate forces (ADDGRID=.TRUE.).

## Acknowledgements

This work has been funded by Research Ireland (Grant Number: 12/RC/2275 P2). DMH is funded by a University of Galway Hardiman Scholarship. ARP acknowledges the Royal Society Olga Kennard fellowship (URF\R1\221067) and JMS acknowledges the UKRI Future Leaders Fellowship ((MR/T043121/1)). PF thanks the research grant from Research Ireland under Grant Number 16/R1/340. The team also acknowledge the Diamond Light Source, beamtime (CY31893–1) for the collection of single crystal structural datasets at the I19 beamline. Open Access funding provided by IReL.

## Conflict of Interests

The authors declare no conflict of interest.

## Data Availability Statement

The data that support the findings of this study are available in the supplementary material of this article.

- [1] H.-C. J. Zhou, S. Kitagawa, *Chem. Soc. Rev.* **2014**, *43*, 5415.
- [2] M. Eddaoudi, D. B. Moler, H. Li, B. Chen, T. M. Reineke, M. O’Keeffe, O. Yaghi, *Acc. Chem. Res.* **2001**, *34*, 319.
- [3] S. Yuan, L. Feng, K. Wang, J. Pang, M. Bosch, C. Lollar, Y. Sun, J. Qin, X. Yang, P. Zhang, Q. Wang, L. Zou, Y. Zhang, L. Zhang, Y. Fang, J. Li, H.-C. Zhou, *Adv. Mater.* **2018**, *37*, 1704303.
- [4] H. Furukawa, K. E. Cordova, M. O’Keeffe, O. M. Yaghi, *Science* **2013**, *341*, 1230444.
- [5] V. F. Yusuf, N. I. Malek, S. K. Kailasa, *ACS Omega* **2022**, *49*, 44507.
- [6] A. E. Thorarinsdottir, T. David Harris, *Chem. Rev.* **2020**, *120*, 8716.
- [7] G. Minguez-Espallargas, E. Coronado, *Chem. Soc. Rev.* **2018**, *47*, 533.
- [8] H. H. Do, S. Y. Kim, *Symmetry* **2023**, *15*, 1830.
- [9] a) M. S. Khan, Y. Li, D.-S. Li, J. Qiu, X. Xu, H. Y. Yang, *Nanoscale Advances* **2023**, *5*, 6318; b) R. Sen, D. K. Hazra, M. Mukherjee, S. Koner, *Eur. J. Inorg. Chem.* **2011**, *18*, 2826; c) H. Chen, S. Liu, Q.-P. Qin, X. Zhang, *ACS Appl. Mater. Interfaces* **2022**, *14*, 18589.
- [10] a) Y.-B. Huang, J. Liang, X.-S. Wang, R. Cao, *Chem. Soc. Rev.* **2017**, *3*, 126; b) R. Sen, D. Saha, S. Koner, *Catal. Lett.* **2012**, *142*, 124; c) Z.-F. Wang, C. Li, Q.-P. Qin, S. Zhang, X. Zhang, *ACS Appl. Nano Mater.* **2023**, *6*, 23430; d) Y.-T. Zheng, S. Li, N.-Y. Huang, X. Li, Q. Xu, *Coord. Chem. Rev.* **2024**, *510*, 215858.
- [11] K. D. J. Hindricks, V. Bon, O. Treske, A. Hannebauer, A. Schaate, Y. Krisiak, S. Kaskel, *Chem. Mater.* **2024**, *36*, 657.
- [12] P. Silva, S. M. Vilela, J. P. C. Tomé, F. A. Almeida Paz, *Chem. Soc. Rev.* **2015**, *7*, 6774.
- [13] R.-B. Lin, S. Xiang, B. Li, Y. Cui, G. Qiann, W. Zhou, B. Chen, *Coord. Chem. Rev.* **2019**, *384*, 21.
- [14] J. Yang, D. Dai, X. Zhang, L. Teng, L. Ma, Y.-W. Yang, *Theranostics* **2023**, *13*, 295.
- [15] Y. Cui, J. Zhang, H. He, G. Qian, *Chem. Soc. Rev.* **2018**, *47*, 5740.
- [16] D. Ma, G. Wang, J. Lu, X. Zeng, Y. Cheng, Z. Zhang, N. Lin, Q. Chen, *Eur. J. Med. Chem.* **2023**, *261*, 115884.
- [17] M. Fytory, K. K. Arafa, W. M. A. El Roubay, A. A. Farghali, M. Abdel-Hafiez, I. M. El-Sherbiny, *Scientific Reports* **2021**, *11*, 19808.
- [18] J. Liu, J. Huang, L. Zhang, J. Lei, *Chem. Soc. Rev.* **2021**, *50*, 1188.
- [19] L. Dai, M. Yao, Z. Fu, X. Li, X. Zheng, S. Meng, Z. Yuan, K. Cai, H. Yang, Y. Zhao, *Nat. Commun.* **2022**, *13*, 2688.

- [20] E. Echenique-Errandonea, R. F. Mendes, F. Figueira, D. Choquesillo-Lazarte, G. Beobide, J. Cepeda, D. Ananias, A. Rodriguez-Dieguez, F. A. Almeida-Paz, J. M. Seco, *Inorg. Chem.* **2022**, *61*, 12977.
- [21] Y. Zhang, S. Liu, Z.-S. Zhao, Z. Wang, R. Zhang, L. Liu, Z.-B. Han, *Inorg. Chem. Front.* **2021**, *8*, 590.
- [22] X. Yu, A. A. Ryadun, D. I. Pavlov, T. Y. Guseynikova, A. S. Potapov, V. P. Fedin, *Angew. Chem. Int. Ed.* **2023**, *62*, e2023306680.
- [23] S. Sun, Y. Zhao, J. Wang, R. Pei, *J. Mat. Chem. B* **2022**, *10*, 9535.
- [24] P. Cheng, *Lanthanide Metal-Organic Frameworks*, Springer, **2015**.
- [25] G. Tan, R.-Q. Jia, W.-L. Wu, B. Li, L.-Y. Wang, *Cryst Growth Des.* **2022**, *22*, 323.
- [26] R. H. Alzard, L. A. Siddig, N. Saleh, H. L. Nguyen, Q. A. T. Nguyen, T. H. Ho, V. Q. Bui, K. Sethupathi, P. K. Sreejith, A. Alzamy, *Sci. Rep.* **2022**, *12*, 18812.
- [27] X. Liu, W. Liu, Y. Kou, X. Yang, Z. Ju, W. Liu, *Inorg. Chem. Front.* **2022**, *9*, 4065.
- [28] X. Wang, K. Batra, G. Clavier, G. Maurin, B. Ding, A. Tissot, C. Serre, *Chem. Eur. J.* **2022**, *29*, e202203136.
- [29] X. Zhai, Y. Kou, L. Liang, P. Liang, P. Sru, Y. Tang, *Inorg. Chem.* **2023**, *62*, 18533.
- [30] S.-N. Zhao, G. Wang, D. Poelman, P. Van Der Voort, *Materials* **2018**, *11*, 572.
- [31] X.-N. Zhang, B.-C. Chen, J.-L. Zhang, J.-L. Zhang, S.-J. Liu, H.-R. Wen, *Dalton Trans.* **2022**, *51*, 15762.
- [32] Z. Li, A. Arauzo, J. G. Planas, E. Bartolome, *Dalton Trans.* **2024**, *53*, 8969.
- [33] I. Aratani, Y. Horii, D. Takajo, Y. Kotani, H. Osawa, T. Kajiwara, *J. Mater. Chem. C* **2023**, *11*, 2082.
- [34] W. J. Rieter, K. M. L. Taylor, H. An, W. Lin, W. Lin, *J. Am. Chem. Soc.* **2006**, *128*, 9024.
- [35] J. Tang, Y. Sheng, H. Hu, Y. Shen, *Prog. Pol. Sci.* **2013**, *38*, 462.
- [36] A. Foucault-Collet, K. A. Gogick, K. A. White, S. Petoud, *PNAS* **2013**, *110*, 17199.
- [37] M. J. Manos, E. J. Kyprianidou, G. S. Papaefstathiou, A. J. Tasiopoulos, *Inorg. Chem.* **2012**, *51*, 6308.
- [38] E. Neofotistou, C. Malliakas, P. Trikalitis, *CrystEngComm* **2010**, *12*, 1034.
- [39] E. J. Kyprianidou, T. Lazarides, S. Kaziannis, C. Kosmidis, G. Itskos, M. J. Manos, A. J. Tasiopoulos, *J. Mater. Chem. A* **2014**, *2*, 5258.
- [40] A. Ahmed, D. McHugh, C. Papatriantafyllopoulou, *Molecules* **2022**, *27*, 6585.
- [41] M. J. Manos, M. S. Markoulides, C. D. Malliakas, G. S. Papaefstathiou, N. Chronakis, M. G. Kanatzidis, P. N. Trikalitis, A. J. Tasiopoulos, *Inorg. Chem.* **2011**, *50*, 11299.
- [42] M. S. Markoulides, C. G. Efthymiou, A. J. Tasiopoulos, N. Chronakis, *SynLett* **2015**, *26*, 2659.
- [43] M. Winterlich, C. G. Efthymiou, W. Papawassiliou, J. P. Carvalho, A. J. Pell, J. Mayans, A. Escuer, M. P. Carty, P. McArdle, E. Tylanakis, L. Morrison, G. Froudakis, C. Papatriantafyllopoulou, *Mater. Adv.* **2020**, *1*, 2248.
- [44] M. Winterlich, D. McHugh, E. O'Toole, K. Skordi, C. O'Malley, R. Sanii, A. Tasiopoulos, A. Erxleben, J. Mayans, L. Morrison, P. McArdle, M. J. Zaworotko, E. Tylanakis, G. Froudakis, C. Papatriantafyllopoulou, *Dalton Trans.* **2021**, *50*, 6997.
- [45] A. Ahmed, C. G. Efthymiou, R. Sanii, E. Patyk-Kazmierczak, A. M. Alsharabasy, M. Winterlich, N. Kumar, D. Sensharma, W. Tong, S. Guerin, P. Farras, S. Hudson, D. Thompson, M. J. Zaworotko, A. J. Tasiopoulos, C. Papatriantafyllopoulou, *J. Mater. Chem. B* **2022**, *10*, 1378.
- [46] R. K. London Singh, *J. Dispers. Sci. Technol.* **2016**, *37*, 239.
- [47] A. Ruiz-Martinez, D. Casanova, S. Alvarez, *Chem. - Eur. J.* **2008**, *14*, 1291.
- [48] M. Llunell, D. Casanova, J. Girera, P. Alemany, S. Alvarez, University of Barcelona, Barcelona, Spain *SHAPE*, version 2.0, **2010**.
- [49] a) A. Kumar, K. Banerjee, A. S. Foster, P. Liljeroth, *Nano Lett.* **2018**, *18*, 5596; b) M. J. Velásquez-Hernández, V. B. López-Cervantes, E. Martínez-Ahumada, M. Tu, U. Hernández-Balderas, D. Martínez-Otero, D. R. Williams, V. Martis, E. Sánchez-González, J.-S. Chang, J. S. Lee, J. Balmaseda, R. Ameloot, I. A. Ibarra, V. Jancik, *Chem. Mater.* **2022**, *34*, 669.
- [50] X.-B. Wang, B. Xia, C.-K. Lyu, D. Kim, E. Li, S.-Q. Fu, J.-Y. Chen, P.-N. Liu, F. Liu, N. Lin, *Commun. Chem.* **2023**, *6*, 73.
- [51] T. Hu, W. Zhong, T. Zhang, W. Wang, Z. F. Wang, *Nat. Commun.* **2023**, *14*, 7092.
- [52] M. Hasegawa, H. Ohmagari, H. Tanaka, K. Machida, *JPPC* **2022**, *50*, 100484.
- [53] S. Kumar, G. Gabarró-Riera, A. Arauzo, J. Hrubý, S. Hill, L. Bogani, J. Rubio-Zuazo, J. Jover, E. Bartolomé, C. Sañudo, *J. Mat. Chem. A* **2024**, *12*, 6269.
- [54] M. Orts-Arroyo, R. Rabelo, A. Carrasco-Berlanga, N. Moliner, J. Cano, M. Julve, F. Lloret, G. De Munno, R. Ruiz-García, J. Mayans, J. Martínez-Lillo, I. Castro, *Dalton Trans.* **2021**, *50*, 380.
- [55] J. Mayans, A. Escuer, *Chem. Commun.* **2021**, *57*, 721.
- [56] G. A. Bain, J. F. Berry, *J. Chem. Educ.* **2008**, *85*, 532.
- [57] O. V. Dolomanov, L. J. Bourhis, R. J. Gildea, J. A. K. Howard, H. Puschmann, *J. Appl. Cryst.* **2009**, *42*, 339.
- [58] G. M. Sheldrick, *Acta Cryst.* **2015**, *A71*, 3.
- [59] G. Kreese, J. Hafner, *Phys. Rev. B* **1993**, *47*, 558.
- [60] J. P. Perdew, K. Burke, M. Ernzerhof, *Phys. Rev. Lett.* **1996**, *77*, 3865.
- [61] S. Grimme, J. Antony, S. Ehrlich, H. Krieg, *J. Chem. Phys.* **2010**, *132*, 154104.
- [62] P. E. Blochl, *Phys. Rev. B* **1994**, *50*, 17953.
- [63] G. Kreese, D. Joubert, *Phys. Rev. B* **1999**, *59*, 1758.
- [64] A. Togo, I. Tanaka, *Scripta Materialia* **2015**, *108*, 1.
- [65] M. Gajdos, K. Hummer, G. Kreese, J. Furthmuller, F. Bechstedt, *Phys. Rev. B* **2006**, *73*, 045112.
- [66] J. M. Skelton, L. A. Burton, A. J. Jackson, F. Oba, S. C. Parker, A. Walsh, *Phys. Chem. Chem. Phys.* **2017**, *19*, 12452.

Manuscript received: August 20, 2024  
Revised manuscript received: December 13, 2024  
Accepted manuscript online: December 16, 2024  
Version of record online: December 23, 2024